PERGAMON

International Journal of Heat and Mass Transfer 42 (1999) 2823–2836

International Journal of HEAT and MASS TRANSFER

Particle dispersion in forced isotropic low-Mach-number turbulence

F. Mashayek[a,*], F.A. Jaberi[b]

[a] *Department of Mechanical Engineering, University of Hawaii at Manoa, 2540 Dole Street, Honolulu, HI 96822-2382, U.S.A.*
[b] *Department of Mechanical and Aerospace Engineering, State University of New York at Buffalo, Buffalo, NY 14260-4400, U.S.A.*

Received 1 June 1998; in final form 20 October 1998

Abstract

Dispersion of solid particles in forced isotropic low-Mach-number turbulent flows is studied. The carrier phase is considered in the Eulerian frame and is simulated by direct numerical simulation (DNS) whereas the particles are treated in a Lagrangian context. The formulation includes the effects of the two-way coupling on the carrier phase. The results verify previous observations for velocity field in similar studies in incompressible flows while providing new insights into the modifications of the thermodynamic fields. It is found that the ratio of the root mean square (rms) Mach number to the mean Mach number is nearly constant (~ 0.41) for all of the cases. A peak value is observed in the variation of the particle velocity variance (normalized with the fluid velocity variance) with the mass loading ratio. The polytropic coefficient decreases linearly by the increase of the mass loading ratio, and nonlinearly by the decrease of the particle time constant.

Nomenclature

C_s specific heat of the solid particle
C_p specific heat of the carrier phase
d_p particle diameter
E_I $p/(\gamma-1)$ internal energy of the carrier phase
E_K $\rho u_i u_i/2$ kinetic energy of the carrier phase
E_T E_I+E_K total energy of the carrier phase
$E(k)$ energy spectrum
f $1+0.15Re_p^{0.687}$
$\mathscr{F}_i$ a zero-mean solenoidal random force
g $Nu/3Pr\,\sigma$
k wavenumber
l $(\pi/2\tilde{u}^2)\int_0^\infty [E(k)/k]\,dk$ integral length scale
L_f reference length
L_v latent heat of vaporization of the liquid
m_p mass of the particle
M_f $u_f/\sqrt{\gamma RT_f}$ reference Mach number
n polytropic coefficient
n_p number of particles within the cell volume
N number of collocation points in each direction
N_p total number of particles
Nu $2+0.6Re_p^{0.5}\,Pr^{0.33}$ Nusselt number
p pressure of the carrier phase
Pr $C_p\mu/\kappa$ Prandtl number
R gas constant
Re_f $\rho_f U_f L_f/\mu$ reference Reynolds number
Re_p $Re_f\rho^* d_p|u_i^*-v_i|$ particle Reynolds number
Re_λ $\rho\tilde{u}\lambda/\mu$ Taylor microscale Reynolds number
S_{ij} $\frac{1}{2}(\partial u_i/\partial x_j+\partial u_j/\partial x_i)$ rate-of-strain tensor
$\mathscr{S}_{ui}$, $\mathscr{S}_{KE}$, $\mathscr{S}_{IE}$ coupling source/sink terms
t time
T temperature
u_i velocity of the carrier phase in direction x_i ($i=1,2,3$)
$\tilde{u}$ turbulence intensity of the carrier phase
U_f reference velocity
v_i velocity of the particle in the direction x_i
x_i spatial coordinates, $i=1,2,3$
X_i position of the particle, $i=1,2,3$.

Greek symbols
γ ratio of the specific heats of the carrier gas

* Corresponding author. Tel.: 001 808 956 9693; fax: 001 808 956 2373; e-mail: mashaye@wiliki.eng.hawaii.edu

0017–9310/99/$ - see front matter
PII: S0017–9310(98)00367–6

δ_{ij} Kronecker delta function
δx node spacing
δV $(\delta x)^3$ cell volume
Δ $\partial uj_j/\partial x_j$ dilatation
ε dissipation rate
η Kolmogorov length scale
κ thermal conductivity of the carrier phase
λ Taylor length scale
μ viscosity of the carrier phase
ρ density
σ C_s/C_p ratio of the specific heats of the two phases
τ_e $l/\tilde{u}$ eddy turnover time
τ_k Kolmogorov timescale
τ_p $Re_f \rho_p d_p^2/18$ particle time constant
ϕ_m mass loading ratio
Φ_p viscous dissipation due to drag
ω_i vorticity component in the direction x_i.

Subscripts
f reference properties for normalization
p particle
rms root mean square
0 value from the one-way coupling simulation.

Superscripts
′ fluctuating quantity
* carrier phase properties at the particle location.

Symbols
$\langle\ \rangle$ Eulerian ensemble average over the number of collocation points
$\langle\langle\ \rangle\rangle$ Lagrangian ensemble average over the number of particles
| conditional distribution
— time average.

1. Introduction

Particle-laden turbulent flows have received a great deal of attention in recent decades [1, 2]. This has been due to both interesting fundamental issues arisen in these flows as well as their significant role in a variety of problems such as spray combustion and atmospheric pollution. From a theoretical point of view, the study of turbulent flows laden with particles is one of the most challenging problems in science. This is primarily due to the fact that the phenomenon of turbulence itself has remained one of the biggest mysteries in science, after more than a century of extensive research. With the addition of particles to a turbulent flow, the additional physical complexities due to multiphase transport including the couplings between the various phases, make the mathematical description of the problem very complex.

Due to its physical nature, the mechanism of dispersion is best understood when analyzed in the 'Lagrangian' context [3, 4]. This makes investigation via numerical simulations very convenient. Several numerical studies of particle-laden turbulent flows have appeared in the literature in recent years with most of the studies concentrated on the dispersion of solid particles in incompressible flows (see [2, 5] for recent reviews). On the other hand, the literature is very rich in both theoretical and computational studies of single-phase compressible flows. An extensive review of the previous works is not intended here; we refer to Blaisdell et al. [6] for a recent review. There have been major developments in numerical studies of single-phase compressible flows during the past few years. Both high-order finite difference [7] and spectral collocation [6, 8–10] methods have been utilized for numerical simulations. These recent studies have significantly enhanced our physical understanding of these flows, providing an appropriate ground for numerical studies of particle dispersion in compressible turbulent flows. Understandably, the extent of previous studies of particle dispersion in compressible turbulent flows is limited. One of the early studies is by Samimy and Lele [11] who consider the motion of heavy particles in a compressible free shear and show that, for the range of convective Mach numbers between 0.2 and 0.6, compressibility does not significantly affect the motion of the particles.

In a previous work [12] we studied the dispersion and polydispersity of evaporating droplets in a forced low-Mach-number turbulence. Here, we consider a similar flow configuration for solid particles and investigate the effects of the two-way coupling on various statistics of the two-phase flow. The objective is to perform a parametric study by considering a reasonable range of variations for particle time constant and mass loading ratio. Since a large number of simulations must be considered, we limit our study to low Reynolds numbers such that the flow can be resolved using 48^3 and 64^3 grid points. A study of high compressibility effects is not intended here and the mean turbulence Mach number is less than 0.2 for all of the cases. At these low Mach numbers, many features of the velocity field are similar to those previously observed in incompressible flows. While comparisons made with previous studies indicate the validity of the results generated here, by considering wider ranges of variation for parameters we are able to expand the previous findings on the velocity fields and to extract new conclusions. The results presented of the thermodynamic fields, however, are to be considered as the main contribution of this study. In Section 2 the problem formulation is presented followed by an overview of the numerical methodology and the simulations. The quasi-stationary turbulence achieved by forcing the low wavenumbers of the flow is discussed in Section 3. A statistical analysis of the results is presented in Section 4 followed by concluding remarks in Section 5.

2. Formulation and methodology

The carrier phase is considered to be a compressible and Newtonian gas with zero bulk viscosity, and to obey the perfect gas equation of state. The Eulerian forms of the non-dimensional continuity, momentum, and energy equations for the carrier phase are:

$$\frac{\partial \rho}{\partial t}+\frac{\partial}{\partial x_j}(\rho u_j)=0 \tag{1}$$

$$\frac{\partial}{\partial r}(\rho u_i)+\frac{\partial}{\partial x_j}(\rho u_i u_j) = -\frac{\partial p}{\partial x_i}+\frac{2}{Re_{\mathrm{f}}}\frac{\partial}{\partial x_j}\left(S_{ij}-\frac{1}{3}\Delta\delta_{ij}\right)+\rho\mathscr{F}_i+\mathscr{S}_{ui} \tag{2}$$

$$\frac{\partial}{\partial t}(E_{\mathrm{T}})+\frac{\partial}{\partial x_j}[u_j(E_{\mathrm{T}}+p)]=\frac{1}{M_{\mathrm{f}}^2\,Pr\,Re_{\mathrm{f}}(\gamma-1)}\frac{\partial^2 T}{\partial x_j\partial x_j} +\frac{2}{Re_{\mathrm{f}}}\frac{\partial}{\partial x_j}\left[u_i\left(S_{ij}-\frac{1}{3}\Delta\delta_{ij}\right)\right]+\rho u_i\mathscr{F}_i+\mathscr{S}_{\mathrm{KE}}+\mathscr{S}_{\mathrm{IE}} \tag{3}$$

accompanied by the equation of state $p=\rho T/\gamma M_{\mathrm{f}}^2$. In (2) and (3), $\mathscr{F}_i$ is a zero-mean and solenoidal random force employed to achieve a quasi-stationary turbulence (discussed in Section 3). All of the variables are normalized by reference length, density, velocity, and temperature scales.

The particles are assumed to be spherical with diameter smaller than the smallest length scale of the turbulence and to exhibit an empirically corrected Stokesian drag force. The rotation of the particles and the gravity effects are neglected. The density of the particles is considered to be constant and much larger than the density of the gas phase such that only the inertia and the drag forces are significant to the particle dynamics. In addition, the particle volume fraction is assumed to be relatively small and both particle–particle interactions and heat transfer due to radiation are neglected. The particles are tracked individually in a Lagrangian manner, and the particle position, velocity, and temperature, respectively, are determined from [13]:

$$\frac{\mathrm{d}X_i}{\mathrm{d}t}=v_i \tag{4}$$

$$\frac{\mathrm{d}v_i}{\mathrm{d}t}=\frac{f}{\tau_{\mathrm{p}}}(u_i^*-v_i) \tag{5}$$

$$\frac{\mathrm{d}T_{\mathrm{p}}}{\mathrm{d}t}=\frac{g}{\tau_{\mathrm{p}}}(T^*-T_{\mathrm{p}}). \tag{6}$$

The particle variables are normalized using the same reference scales as those used for the gas phase variables. The function $f=1+0.15Re_{\mathrm{p}}^{0.687}$ in (5) represents an empirical correction to the Stokes drag due to particle Reynolds numbers of order unity and larger [14] and is valid for particle Reynolds numbers $Re_{\mathrm{p}}\leqslant 1000$. The particles are assumed 'lumped', so that there is no temperature variation within each particle. The right-hand side of (6) represents the rate of change of the particle temperature due to convective heat transfer with the surrounding gas. The factor $g=Nu/3Pr\,\sigma$ represents a correlation for the convective heat transfer coefficient based on an empirically corrected Nusselt number ($Nu=2+0.6Re_{\mathrm{p}}^{0.5}\,Pr^{0.33}$) [15].

The source/sink terms $\mathscr{S}_{ui}$, $\mathscr{S}_{\mathrm{KE}}$, and $\mathscr{S}_{\mathrm{IE}}$ appearing in (2) and (3) represent the integrated effects of the particles on the momentum, kinetic energy, and internal energy of the gas, respectively. These Eulerian fields are calculated from the Lagrangian particle variables by volume averaging the contributions from all of the individual particles residing within the cell centered around each grid point:

$$\mathscr{S}_{ui}=-\frac{1}{\delta V}\sum^{n_{\mathrm{p}}}\frac{fm_{\mathrm{p}}}{\tau_{\mathrm{p}}}(u_i^*-v_i) \tag{7}$$

$$\mathscr{S}_{\mathrm{KE}}=-\frac{1}{\delta V}\sum^{n_{\mathrm{p}}}\frac{fm_{\mathrm{p}}}{\tau_{\mathrm{p}}}(u_i^*-v_i)u_i^* \tag{8}$$

$$\mathscr{S}_{\mathrm{IE}}=-\frac{\sigma}{(\gamma-1)M_{\mathrm{f}}^2\delta V}\sum^{n_{\mathrm{p}}}\frac{gm_{\mathrm{p}}}{\tau_{\mathrm{p}}}(T^*-T_{\mathrm{p}})+\Phi_{\mathrm{p}}. \tag{9}$$

In (9), $\Phi_{\mathrm{p}}=(1/\delta V)\,\Sigma^{n_{\mathrm{p}}}\{(fm_{\mathrm{p}}/\tau_{\mathrm{p}})\,(u_i^*-v_i)^2\}$ is the viscous dissipation due to drag. This term contributes to the change of the internal energy and is distinguished from the contribution of the drag force to the kinetic energy [given by (8)]. A more elaborate physical discussion for Φ_{p} may be found in [16].

Simulations are conducted within the domain $0\leqslant x_i\leqslant 2\pi$. A Fourier pseudospectral [17] method with triply periodic boundary conditions is employed for the spatial discretization of all transport variables. The nonlinear terms are calculated in physical space where all of the variables are stored, and spatial differentiations are performed in Fourier space. Aliasing errors are treated by truncating energies outside of a spherical wavenumber shell having radius $\sqrt{2}N/3$. Time advancement for both the Eulerian gas equations and the Lagrangian particle equations is performed using an explicit second order accurate Adams–Bashforth scheme. Calculation of the values of the Eulerian gas variables at the particle locations is by a fourth-order Lagrange polynomial interpolation scheme. To emulate the stationary isotropic turbulence field, a low wavenumber forcing scheme is imposed. The forcing algorithm employed is based on a scheme developed by Eswaran and Pope [18]. A forcing acceleration term ($\mathscr{F}_i$) is added to the momentum equations and is limited to a low wavenumber shell. The acceleration vector at each forced node is comprised of six independent random variables having Gaussian distribution with zero mean and unity variance. The three complex random vectors are made solenoidal in the same

manner as described in [18] and correspond to their zero time scale case (white noise in time). The relative strength of the forcing is a function of the reference Reynolds number Re_f and the variance of the components of the random vectors.

The performance of the code for the Navier–Stokes equations (on a Cray-C90) is approximately 4.0 s per time-step for simulations with resolutions of 64^3 grid points. Numerical integration of 5.5×10^5 particles with only one-way coupling ($\mathscr{S}_{ui}$, $\mathscr{S}_{KE}$, $\mathscr{S}_{IE}\equiv 0$) requires an additional 2.75 s per time-step, while the additional time for a full two-way coupling simulation is 4.7 s per iteration. The time for integrating the particles scales approximately linearly with the number of particles. The simulations are performed employing both 48^3 and 64^3 collocation points. Tables 1 and 2 provide a listing of different cases considered for this study. The simulations with 48^3 collocation points are intended to investigate the effects of the particle time constant (τ_p) and the ratio of the particle specific heat coefficient to that of the gas (σ). These simulations are also used to compare the effects of one-way and two-way couplings. The 64^3 simulations are used to study the effects of the mass loading ratio (ϕ_m) and to generate the particle concentration related statistics which require high resolution. In order to investigate the effects of Φ_p, several cases from Table 1 are repeated with $\Phi_p = 0$ (these cases are not listed in Table 1 for brevity). All of the simulations use $Pr = 0.7$ and $M_f = 1$. With this value for M_f, the speed of sound based on the initial mean gas temperature is the reference scale for the velocity.

A study of high compressibility effects is not intended in this work and the mean turbulence Mach number is kept less than 0.2 for all of the cases. At this mean Mach number the flow is completely free of shocks, therefore, 48^3 and 64^3 collocation points suffice to accurately resolve the flow field. This is evident by high values of $\bar{\eta}k_{max}$ (k_{max} is the highest resolved wavenumber) in Tables 1 and 2. The values of $d_p/\bar{\eta}$ indicate that the sizes of the particles are sufficiently smaller than the smallest scales of the flow and satisfy the assumption made in using the Stokesian drag for the particle momentum equation. Other par-

Table 1
Parameters used in the 48^3 simulations; $Re_f = 350$

τ_p	ϕ_m	N_p	ρ_p	σ	Coupling	$\overline{Re_\lambda}$	$\bar{\tau}_e$	$\tau_p/\bar{\tau}_k$	$d_p/\bar{\eta}$	$\bar{\eta}k_{max}$
0	—	50 000	1000	—	—	28.0	16.7	0	0	1.83
2	—	227 070	1000	1	1-way	28.0	16.7	0.83	0.123	1.83
4	—	80 281	1000	1	1-way	28.0	16.7	1.66	0.173	1.83
8	—	28 384	1000	1	1-way	28.0	16.7	3.32	0.245	1.83
12	—	15 450	1000	1	1-way	28.0	16.7	4.98	0.300	1.83
2	0.5	227 070	1000	1	2-way	25.7	24.9	0.56	0.101	2.22
4	0.5	80 281	1000	1	2-way	26.9	25.3	1.08	0.140	2.27
8	0.5	28 384	1000	1	2-way	27.4	25.0	2.13	0.196	2.28
12	0.5	15 450	1000	1	2-way	27.3	24.4	3.24	0.242	2.26
2	0.5	227 070	1000	4	2-way	25.7	24.9	0.56	0.101	2.22
4	0.5	80 281	1000	4	2-way	26.9	25.3	1.08	0.140	2.27
8	0.5	28 384	1000	4	2-way	27.4	25.0	2.13	0.196	2.28
12	0.5	15 450	1000	4	2-way	27.3	24.4	3.24	0.242	2.26

Table 2
Parameters used in the 64^3 simulations; $Re_f = 400$

τ_p	ϕ_m	N_p	ρ_p	σ	Coupling	$\overline{Re_\lambda}$	$\bar{\tau}_e$	$\tau_p/\bar{\tau}_k$	$d_p/\bar{\eta}$	$\bar{\eta}k_{max}$
2	—	554 852	1000	1	1-way	36.7	14.5	1.01	0.135	2.18
2	0.1	55 485	1000	1	2-way	34.5	16.9	0.86	0.124	2.29
2	0.25	138 713	1000	1	2-way	33.4	18.7	0.78	0.119	2.40
2	0.5	277 426	1000	1	2-way	30.1	22.8	0.65	0.108	2.62
2	1.0	554 852	1000	1	2-way	24.9	26.9	0.57	0.102	2.80
3	0.25	138 713	3375	1	2-way	33.5	19.0	1.13	0.078	2.44
5	—	140 368	1000	1	1-way	36.7	14.5	2.53	0.213	2.18
5	1.0	140 368	1000	1	2-way	28.9	25.8	1.44	0.161	2.80

ameters shown in Tables 1 and 2, are the total number of the particles (N_p), the ratio of the particle time constant to the time averaged Kolmogorov time scale ($\bar{\tau}_k$), the time averaged eddy-turnover time ($\bar{\tau}_e$), and the time averaged Reynolds number based on the Taylor length scale ($\overline{Re_\lambda}$). Noticeable in Table 1, is the insensitivity of the velocity field of the carrier phase to the variation of σ. Therefore, in the discussion of the results, only the effects of σ on the thermodynamic fields are considered.

3. Quasi-stationary turbulence

Before analyzing the results, it is instructive to discuss the state of stationarity achieved (for both the flow and the particles) with the numerical technique of Section 2. The flow is forced externally and the energy due to external forcing is input at low wavenumbers and then follows an energy cascade towards the small scales where it is dissipated into heat. In this manner, a stationary state is reached for the kinetic energy (after an initial transient period), however, the internal energy of the gas continuously increases in time as the simulation box (due to homogeneity) has no net heat transfer with the surrounding. Therefore, only a 'quasi-stationary' state is obtained for the kinetic energy [8]; this is discussed (via DNS results) in detail below.

Shown in Fig. 1 are the temporal variations of the mean temperatures of the gas and the particles for a variety of cases with $\phi_m = 0.5$ and $\tau_p = 2$. Time is normalized by the eddy-turn-over time of the single-phase flow ($\bar{\tau}_{e0}$), and the particles are randomly distributed at $t = 0$ with the same velocity and temperature as those of the local gas. For the case with one-way coupling, Fig. 1(a) shows that the gas temperature increases in time due to the forcing energy which is transformed into the internal energy by viscous dissipation and pressure-dilatation correlation. A portion of the gas internal energy is transferred to the particles and results in the increase of the dispersed phase mean temperature as shown in Fig. 1(b). For the case with two-way coupling, having the same value for σ as in the case with one-way coupling, also an increase in the temperature of the gas and the particles is observed but after an initial transient period during which the mean temperature rises fast. The initially fast increase in the gas temperature is explained by considering that the particles are injected at the same velocity as that of the local gas at $t = 0$. In the stationary state (long times), the particle velocity lags the gas velocity due to the particle inertia, therefore, part of the initial kinetic energy of the particles is transferred to the gas and is dissipated into heat.

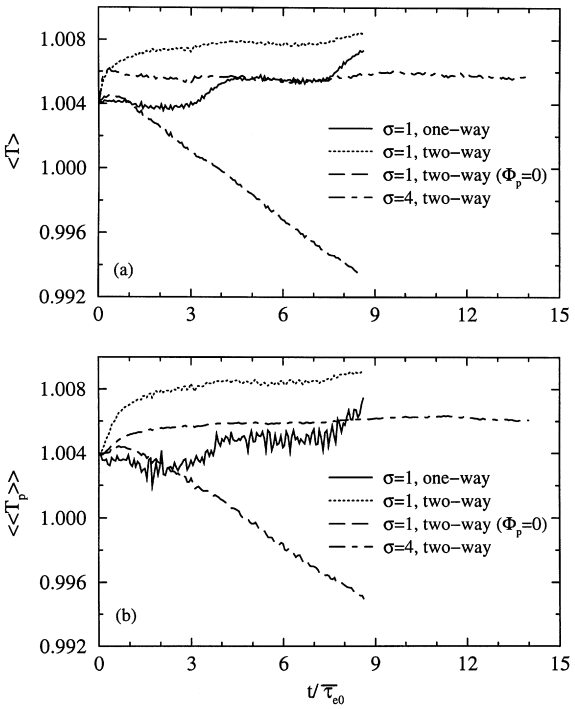

Fig. 1. Temporal variations of the mean temperatures of (a) the carrier and (b) the dispersed phases. For all of the cases $\phi_m = 0.5$ and $\tau_p = 2$.

In order to investigate the significance of the internal energy production by drag (Φ_p) a similar two-way coupling case but with $\Phi_p = 0$ is considered. Figure 1 indicates that turning the Φ_p term off, results in a decreasing trend for the temperature and, consequently, the internal and the total energies of both phases. The results of additional simulations (not shown) indicated that the rate of decrease of the temperature depends on the particle size and increases with the decrease of τ_p. Obviously, the decrease of the total energy is not in agreement with the fact that energy is being added to the system by external forcing, and there is no net heat or work transfer with the gas outside the box. The effect of the increase of the particles heat capacity on the mean temperature is also shown in Fig. 1 by considering the temporal variation of the mean temperature for a case with $\sigma = 4$. Recall that σ represents the ratio of the particle specific heat (C_s) to that of the gas (C_p); therefore, an increase in σ can be interpreted as an increase in C_s while C_p is kept constant. By increasing C_s, a larger portion of the gas internal energy is consumed to increase the mean temperature of the particles, resulting in the decrease of the mean temperature of both phases.

A close inspection of Fig. 1 indicates that the mean gas temperature is lower than that of the particles. This is despite the fact that the particles can increase their internal energy only by absorbing heat from the gas, and can be explained by considering the types of averaging performed on the gas and the particle temperatures. The mean gas temperature is calculated by Eulerian averaging over the entire simulation box while the particle mean temperature is obtained by Lagrangian averaging over

the number of particles. The correct indicator of the direction of heat transfer, is the 'mean temperature difference' between the particle and its neighboring gas, i.e. $\overline{\langle\langle T^*-T_p\rangle\rangle}$. The calculated values of $\overline{\langle\langle T^*-T_p\rangle\rangle}$ are presented in Table 3 and all of them are positive, thus indicating a heat transfer from the gas to the particles. The mean temperature difference increases with the increase of τ_p regardless of one- or two-way coupling or magnitude of σ. This is due to the larger heat capacity of larger particles and is similar to increase of the mean relative velocity with the increase of particle inertia. Further, cases with two-way coupling exhibit a smaller mean temperature difference in comparison to cases with one-way coupling, as in the former, the particles tend to modify the temperature of the surrounding gas closer to their own temperature. The increase of σ enhances the heat capacity of the particles and a larger heat transfer from the gas is needed to increase the particle temperature. This results in the increase of $\overline{\langle\langle T^*-T_p\rangle\rangle}$ with the increase of σ as indicated in Table 3.

The fact that 'the difference of the mean temperatures', calculated by averaging the gas temperature over the entire box, is smaller than 'the mean temperature difference', obtained from averaging over the particle locations, indicates that the gas elements surrounding the particles are warmer than the gas elements located far from the particles. The reason is that the heat generated by drag (calculated from Φ_p) is added to the gas elements surrounding the particles. Therefore, the gas elements closer to the particles attain higher temperatures than those far from the particles.

Although the mean temperature increases in time, a statistically stationary state is reached for temperature fluctuations (T' and T'_p) after an initial transient period. Figures 2(a) and (b) portray the temporal variation of the root mean square (rms) of the particle fluctuating temperature (T'_{prms}) for $\tau_p = 2$ and $\tau_p = 12$, respectively. Both one- and two-way couplings are considered. It is observed in the figure that all of the cases reach a statistically stationary state at long times. However, the initial period to reach the stationary state varies for different cases. The larger particles need longer transient periods as they have larger heat capacities and, for the same reason, the particles with larger σ take longer to become stationary. A comparison of cases with $\Phi_p = 0$ (not shown) with cases considered in Fig. 2 indicated identical results for fluctuating temperatures. Therefore, neglect of the heat generated by drag has no effect on fluctuating quantities.

Table 3
Values of $\overline{\langle\langle T^*-T_p\rangle\rangle}$ for different cases

τ_p	$\overline{\langle\langle T^*-T_p\rangle\rangle}\times 10^4$		
	$\sigma = 1$, 1-way	$\sigma = 1$, 2-way	$\sigma = 4$, 2-way
2	12.1	1.00	1.25
4	12.9	2.06	2.47
8	14.6	3.87	4.69
12	15.6	5.57	7.04

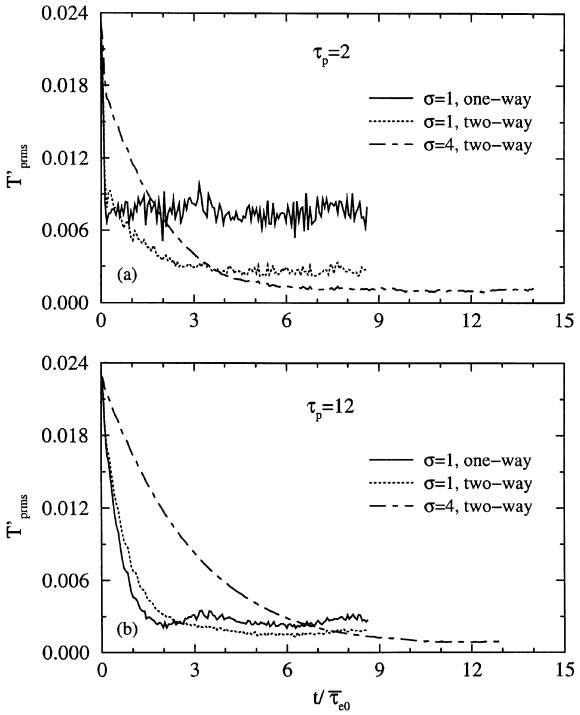

Fig. 2. Temporal variations of the rms of the particle fluctuating temperature for (a) $\tau_p = 2$ and (b) $\tau_p = 12$. For all of the cases $\phi_m = 0.5$.

Also noticeable in Fig. 2 is the damping of the temporal oscillations of rms temperature when the particles are in two-way coupling with the flow. This is explained by considering the temporal variations of the mean pressure–dilatation correlation ($\langle p\Delta\rangle$) appearing in the transport equations for the mean kinetic and internal energy of the carrier phase, respectively, [8, 16]:

$$\frac{\mathrm{d}}{\mathrm{d}t}\langle E_K\rangle = \langle p\Delta\rangle - \varepsilon + \langle \rho u_i \mathscr{F}_i\rangle - \left\langle \frac{1}{\delta V}\sum^{n_p} F_{pi}u_i^* \right\rangle \tag{10}$$

$$\frac{\mathrm{d}}{\mathrm{d}t}\langle E_I\rangle = -\langle p\Delta\rangle + \varepsilon + \left\langle \frac{1}{\delta V}\sum^{n_p} F_{pi}(u_i^* - v_i) \right\rangle + \langle \mathscr{S}_{IE,conv}\rangle. \tag{11}$$

Here, ε is the rate of dissipation of the turbulence kinetic energy at small scales (due to viscosity), $F_{pi} = (fm_p/\tau_p)(u_i^* - v_i)$ is the drag force and $\langle(1/\delta V)\Sigma^{n_p} F_{pi}u_i^*\rangle$, which

we refer to as ε_p, is the rate of dissipation of the gas kinetic energy due to drag. The contribution of Φ_p to change of the internal energy is denoted by $\langle(1/\delta V)\Sigma^{n_p} F_{pi}(u_i^* - v_i)\rangle$, and $\langle \mathscr{S}_{IE,conv}\rangle$ represents the effect of the convective heat transfer.

Equations (10) and (11) show that the pressure–dilatation correlation $\langle p\Delta\rangle$ has no contribution to the change of the total energy of the carrier phase and it only exchanges energy between kinetic and internal modes. It oscillates in time with relatively large amplitude and frequency, therefore, a clearly observable effect of the pressure–dilatation term is the amplification of the temporal oscillations (which are primarily generated by the random forcing) in kinetic and internal energies. Although the time integral of $\langle p\Delta\rangle$ takes small values, the instantaneous local values of $p\Delta$ can be quite large in comparison to the other terms in (10) and (11) [8]. Figure 3(a) depicts a typical temporal variation of the pressure–dilatation correlation calculated from a single-phase flow simulation. In the absence of particles, $\langle p\Delta\rangle$ takes instantaneous values as large as approximately $\pm 3\times 10^{-3}$, however, its time averaged value is less than 10^{-4}. Injecting the particles into the flow decreases both the amplitude of oscillations of $\langle p\Delta\rangle$ and its time averaged value (Fig. 3(b) and (c)). However, a comparison of Fig. 3(b) and (c) indicates that, for the same mass loading ratio, the damping effects of the smaller particles ($\tau_p = 2$) on oscillations of the pressure–dilatation correlation are markedly stronger than those of the larger particles ($\tau_p = 12$). This is due to the fact that at constant mass loading ratio the smaller particles outnumber the larger particles by a factor of about 14 (see Table 1), therefore, the smaller particles are more effective in diminishing the spatial variations of $\langle p\Delta\rangle$. The time averaged value, however, is not as sensitive to the size of the particle and varies by only 25% for cases shown in Fig. 3(b) and (c).

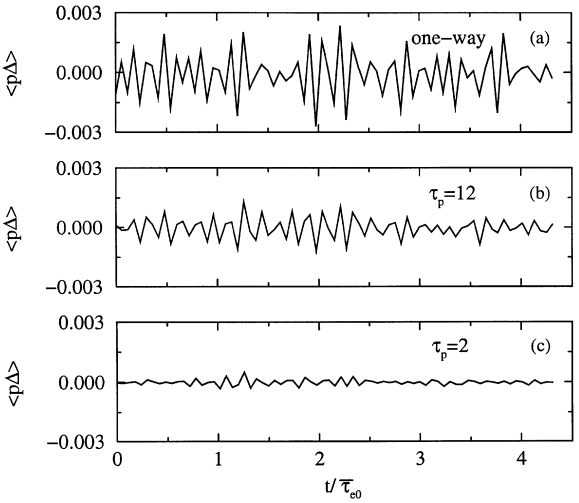

Fig. 3. Temporal variations of the pressure–dilatation correlation for (a) one-way coupling, (b) $\phi_m = 0.5$, $\tau_p = 12$, and (c) $\phi_m = 0.5$, $\tau_p = 2$. For all of the cases $\sigma = 1$.

When using artificially forced flow fields to investigate the effects of the particles on the flow and vice versa, there is always a concern whether or not the energy provided by forcing, remains the same for all of the cases when the mass loading ratio or the particle time constant is varied (e.g. see Elghobashi and Truesdell [19]). To address this issue, we consider the time averaging of equation (10) which yields $\overline{\langle \rho u_i \mathscr{F}_i\rangle} = -\overline{\langle p\Delta\rangle} + \bar{\varepsilon} + \bar{\varepsilon}_p$. To maintain a statistically stationary turbulence, the forcing energy is to be balanced by the sum of the total dissipation ($\bar{\varepsilon} + \bar{\varepsilon}_p$) and the pressure–dilatation correlation. An analysis of the simulations indicated that this sum is almost the same for all of the cases. Therefore, it may be concluded that the time averaged values of the external forcing does not significantly change when the particle time constant or the mass loading ratio is varied.

4. Particle dispersion in stationary turbulence

In this section the effects of the mass loading ratio, the particle time constant, and the particle specific heat on the statistics of the gas and the particles in stationary (or more precisely quasi-stationary) turbulence are studied. Figure 4 portrays the effects of the mass loading ratio and the particle time constant on time averaged values of the turbulence kinetic energy, $\overline{q^2}$ ($=\frac{1}{2}\overline{\rho u_i u_i}$), the rate of dissipation of the turbulence kinetic energy $\bar{\varepsilon}$, the entropy $\bar{e}$ ($=\frac{1}{2}\overline{\omega_i\omega_i}$, ω_i is the vorticity component), the rms density fluctuations, $\overline{\rho'_{rms}}$, the rms pressure fluctuations, $\overline{p'_{rms}}$, the rms temperature fluctuations, $\overline{T'_{rms}}$, and the rms dilatation, $\overline{\Delta_{rms}}$. All of the variables are normalized with their respective values (denoted by subscript 0) from the one-way coupling simulation. Figure 4(a) indicates that all of these variables decrease with the increase of the mass loading ratio. The rate of decrease, however, is different; the smallest rate is for the turbulence kinetic energy and the largest rate is for the dilatation. The large rate of decrease for all of the variables near $\phi_m = 0$ demonstrates the significance of the two-way coupling even for small mass loading ratios. For example, the rms dilatation is decreased by about 50% of its one-way coupling value for a mass loading ratio of 0.1. For the same mass loading ratio, the kinetic energy decreases by 20%. This is larger than the 10% decrease predicted by Squires and Eaton [20] for incompressible flow at the same mass loading ratio. The difference is (likely) not due to the compressibility effects only and other factors such as differences in particle sizes and forcing schemes may have also contributed.

The changes in the particle time constant affect the above-mentioned variables in a different manner. Figure 4(b) shows that the dissipation rate of the turbulence

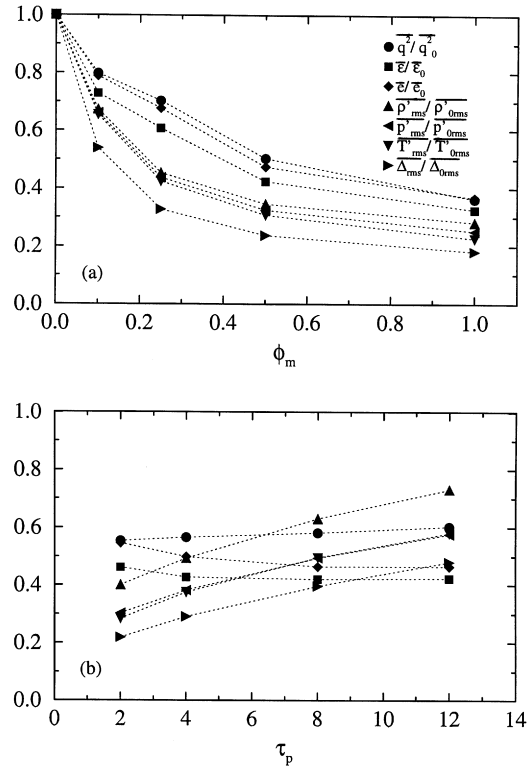

Fig. 4. Variations of the turbulence kinetic energy, the dissipation rate of the turbulence kinetic energy, the entropy, the rms density, the rms pressure, the rms temperature, and the rms dilatation of the gas phase vs. (a) the mass loading ratio and (b) the particle time constant. All of these quantities are normalized with their respective values from one-way coupling cases. Legends are the same in (a) and (b).

kinetic energy, and the entropy first decrease with the increase of τ_p and then level off for larger τ_p values. The turbulence kinetic energy remains virtually unaffected by the change of the particle time constant. The rms of the gas density, pressure, temperature, and dilatation monotonically increase with the increase of τ_p. This can be explained by considering the increase in the number of particles with the decrease of the particle time constant when the mass loading ratio is held constant. In a compressible flow fluctuating quantities such as density, pressure, temperature, and dilatation experience spatial variations. A primary effect of the particles is to diminish these fluctuations. Increasing the number of particles diminishes the fluctuations more uniformly in space.

In compressible flows, the dissipation rate of the turbulence kinetic energy consists of incompressible (or rotational), ε_I, and compressible (or irrotational), ε_C, components [8, 6]:

$$\varepsilon_I = \frac{1}{Re_f}\langle|\omega|^2\rangle, \quad \varepsilon_C = \frac{1}{Re_f}\frac{4}{3}\langle\Delta^2\rangle. \tag{12}$$

Table 4 shows the effects of the mass loading ratio and the particle time constant on the ratio $\bar{\varepsilon}_C/\bar{\varepsilon}_I$. Based on the results shown in Table 4, the contribution of the compressible part diminishes with the increase of the mass loading ratio and/or the decrease of the particle time constant. This is due to the decrease of the velocity dilatation in the presence of the particles as was discussed in Section 3.

An interesting feature is observed in the variations of the mean Mach number ($\langle M\rangle$) and the rms of the fluctuating Mach number ($\overline{M'_{rms}}$) with the mass loading ratio. Figure 5 shows that both the mean and the rms Mach number decrease monotonically with the increase of the mass loading ratio, however, the ratio $\overline{M'_{rms}}/\overline{\langle M\rangle}$ remains unaffected by the change of ϕ_m. As the mean Mach number decreases, due to the effects of the two-

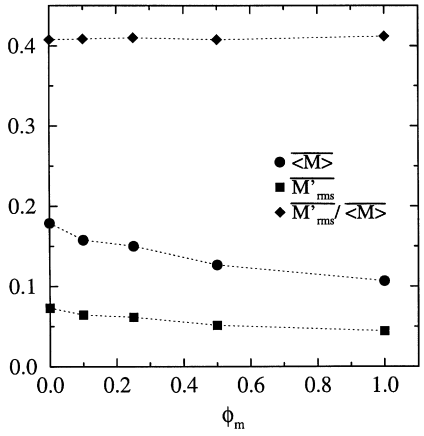

Fig. 5. Variations of the mean Mach number, the rms Mach number, and the ratio of the two vs. the mass loading ratio. For all of the cases $\tau_p = 2$ and $\sigma = 1$.

Table 4
Variations of $\bar{\varepsilon}_C/\bar{\varepsilon}_I$ with the mass loading ratio and the particle time constant

τ_p	2	2	2	2	2	0	2	4	8	12
ϕ_m	0	0.1	0.25	0.5	1.0	0.5	0.5	0.5	0.5	0.5
$\bar{\varepsilon}_C/\bar{\varepsilon}_I$	0.135	0.052	0.022	0.017	0.013	0.214	0.020	0.037	0.074	0.108

way coupling, the fluctuations of the Mach number also decreases proportionally to the decrease of the mean value. This is not, however, the case for other quantities shown in Fig. 4(a). The mean values of the temperature and the pressure change very negligibly in comparison to changes in their fluctuating parts. The mean density and dilatation do not change at all and are constant for all of the cases. A similar behavior for $\overline{M'_{\rm rms}}/\overline{\langle M\rangle}$ was observed with the change of the particle time constant. In fact both the mean and the rms Mach number remain relatively unaffected by changes in $\tau_{\rm p}$. For all of the cases considered here the value of $\overline{M'_{\rm rms}}/\overline{\langle M\rangle}$ was found to be about 0.41. This finding, meaning the constancy of $\overline{M'_{\rm rms}}/\overline{\langle M\rangle}$, can be of great interest in statistical modeling of particle-laden compressible flows with low compressibility effects. Further simulations with higher resolutions are needed to assess this observation at higher Mach numbers.

The particle velocity autocorrelation coefficients are shown in Fig. 6. The autocorrelation coefficient in a direction ξ is defined as (no summation over the repeated Greek indices):

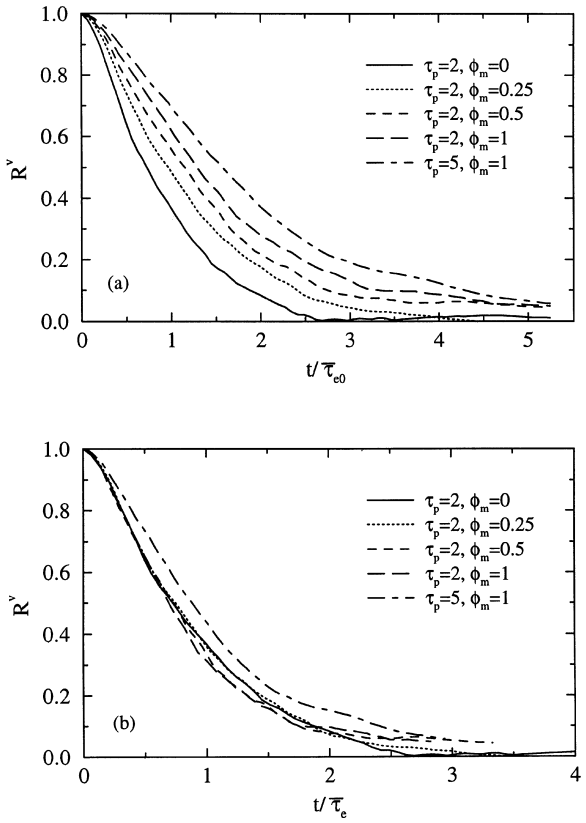

Fig. 6. Variations of the particle velocity autocorrelations at different values of the particle time constant and the mass loading ratio vs. (a) time normalized with the eddy-turn-over time of the one-way coupling case and (b) time normalized with the eddy-turn-over time of the respective case.

$$R^{v}_{\xi\xi}(t)=\frac{\langle\langle v_\xi(\tau)v_\xi(\tau+t)\rangle\rangle}{(\langle\langle v^2_\xi(\tau)\rangle\rangle\langle\langle v^2_\xi(\tau+t)\rangle\rangle)^{0.5}},\quad \xi=1,2,3 \qquad (13)$$

where τ is a time in the stationary state from which calculation of $R^{v}_{\xi\xi}(t)$ is begun. Equation (13) is usually used for non-stationary turbulence; for stationary turbulence the denominator is expressed as $\langle\langle v^2_\xi(\tau)\rangle\rangle$. The difference between the two is very small, however, using (13) decreases the oscillations (due to forcing) of the autocorrelation curves. The autocorrelation coefficients shown on Fig. 6 are the average values over the three directions—these averaged autocorrelations are indicated as R^{v} with no subscript for direction. Figure 6(a) indicates that, for the same $\tau_{\rm p}$ value, the increase of the mass loading ratio increases the velocity autocorrelation coefficient. This has also been observed in incompressible decaying turbulence by Elghobashi and Truesdell [19] who argue that as the mass loading ratio increases the ability of the particles to modify their neighboring gas also increases. Therefore, the difference between the velocity of the gas and that of the particle decreases and the particle velocity is less influenced by the gas. In other words, the change of the particle velocity autocorrelation with the mass loading ratio is due to modification of the turbulence by the particles. As the mass loading ratio increases the gas kinetic energy decreases and the flow becomes more 'sluggish'. This is verified by comparing the eddy-turn-over time ($\bar{\tau}_{\rm e}$) values given in Table 2 which indicates the increase of the eddy-turn-over time with the increase of the mass loading ratio. Based on this observation, a similarity can be expected in the behavior of the velocity autocorrelations if the time for each curve is normalized by its corresponding $\bar{\tau}_{\rm e}$ value from Table 2. Figure 6(b) depicts R^{v} vs. such a normalized time axis, and indicates that the autocorrelation curves for different mass loading ratios closely collapse on one curve. The behavior of the autocorrelation with a larger particle time constant ($\tau_{\rm p}=5$) is different since the increase of R^{v} with the increase of $\tau_{\rm p}$ is due to the inertia effects rather than the turbulence modifications.

In a similar manner, autocorrelation coefficients ($R^{T_{\rm P}}$) are calculated for the fluctuating part of the particle temperature using an equation analogous to (13) with $T'_{\rm p}$ substituted for v_ξ. The temperature autocorrelations are presented in Fig. 7 for a variety of cases. In Fig. 7(a) the effects of the two-way coupling and the particle specific heat are portrayed for $\phi_{\rm m}=0.5$ and $\tau_{\rm p}=12$. Similarly to the velocity autocorrelation, two-way coupling increases the particle temperature autocorrelation by modifying the temperature of the gas surrounding the particle. In two-way coupling, the increase of the particle specific heat (represented by σ) results in a significant increase of the particle temperature autocorrelation. The particle with larger heat capacity has less tendency in changing its temperature than the particle with smaller heat capacity does. This is similar to the effect of inertia on the particle

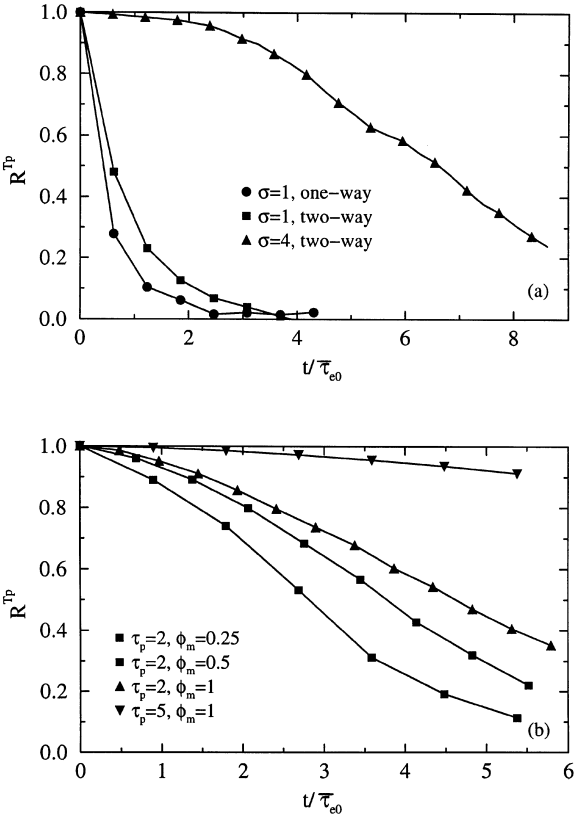

Fig. 7. Temporal variations of the particle temperature autocorrelations. (a) Effects of one- and two-way couplings and particle specific heat at $\phi_m = 0.5$ and $\tau_p = 12$, and (b) effects of mass loading ratio and particle time constant at $\sigma = 1$.

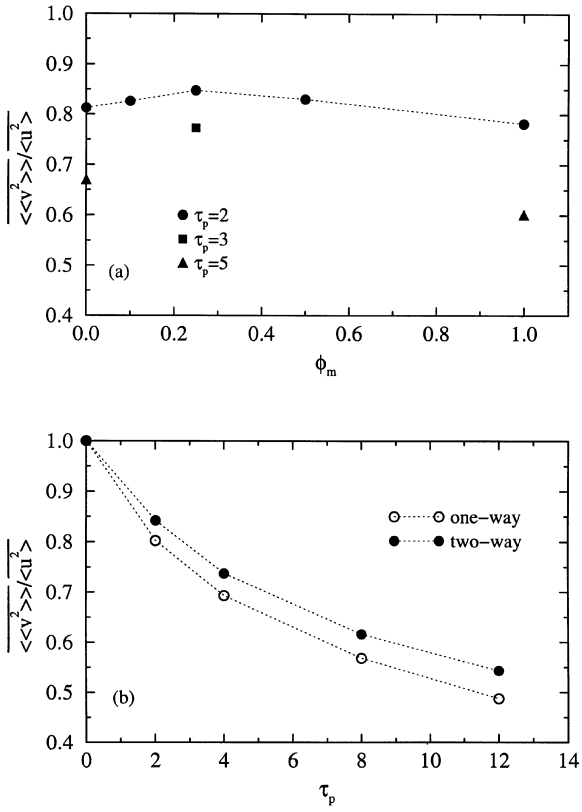

Fig. 8. Variations of the particle velocity variance normalized with the fluid velocity variance vs. (a) the mass loading ratio and (b) the particle time constant.

velocity autocorrelation. Figure 7(b) shows the effects of the mass loading ratio and the particle time constant on R^{T_p} for a constant ratio of the specific heats, $\sigma = 1$. As expected, an increase of the mass loading ratio and/or the particle time constant results in a higher temperature autocorrelation. However, comparison of Figs 6(a) and 7(b) indicates that these effects are more visible in the temperature autocorrelations than in the velocity autocorrelations.

Figure 8 shows the variations of the ratio of the particle velocity variance ($\overline{\langle\langle v^2\rangle\rangle}$) to the gas velocity variance ($\overline{\langle u^2\rangle}$) with the mass loading ratio and the particle time constant. Both $\overline{\langle u^2\rangle}$ and ($\overline{\langle\langle v^2\rangle\rangle}$) are calculated by time averaging over a stationary interval extending more than three eddy-turn-over times. Figure 8(a) indicates a peak in the variation of $\overline{\langle\langle v^2\rangle\rangle}/\overline{\langle u^2\rangle}$ with the mass loading ratio around $\phi_m = 0.25$, when the particle time constant is fixed at $\tau_p = 2$. As the mass loading ratio is increased from zero towards 0.25 the gas turbulence decays more than the particle turbulence. This is in agreement with Fig. 4(a) which indicates a sharp decrease in the gas kinetic energy, $\overline{q^2}$, at small mass loading ratios. For larger values of the mass loading ratio the gas kinetic energy decreases with a smaller rate and the ratio of the particle velocity variance to that of the gas decreases. The effect of the particle time constant on the ratio of the velocity variances is shown in Fig. 8(b) for $\phi_m = 0.5$. As the particle time constant increases the velocity difference between the particle and the gas also increases due to the larger inertia of the larger particle. On the other hand, the gas velocity variance ($\overline{\langle u^2\rangle}$) is not very sensitive to the change of τ_p as witnessed from Fig. 4(b). As a result, the ratio of the particle to the gas velocity variance decreases with the increase of τ_p. Figure 8(b) also provides a comparison between one- and two-way coupling cases, and indicates larger values for $\overline{\langle\langle v^2\rangle\rangle}/\overline{\langle u^2\rangle}$ in two-way coupling.

A similar variation with τ_p is observed for the ratio of the rms of the particle fluctuating temperature to that of the gas ($\overline{T'_{prms}}/\overline{T'_{rms}}$). Figure 9(a) portrays the variation of $\overline{T'_{prms}}/\overline{T'_{rms}}$ with τ_p for two different values of the normalized particle specific heat. A comparison is also made between one- and two-way coupling cases. An increase of τ_p and/or σ enhances the particle heat capacity and

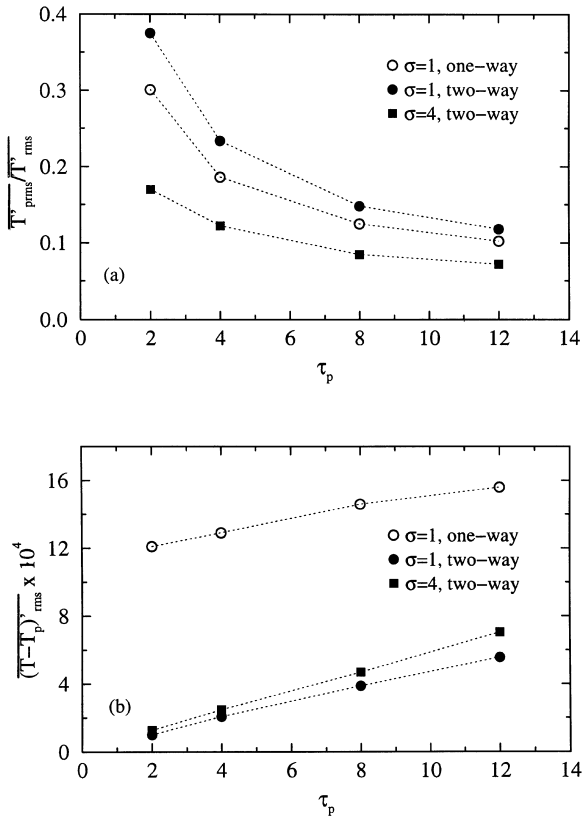

Fig. 9. Variations of (a) the rms of the particle temperature normalized with the rms of the gas temperature and (b) the rms of the temperature difference between the gas and the particles, vs. the particle time constant. For all of the cases $\phi_m = 0.5$.

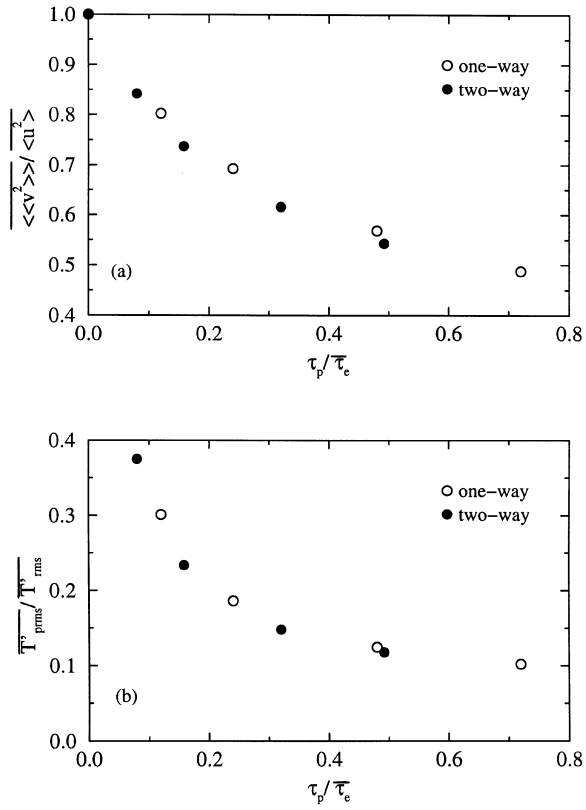

Fig. 10. Variations of (a) the particle turbulence intensity normalized with the gas turbulence intensity and (b) the rms particle temperature normalized with the rms gas temperature vs. the particle time constant normalized with the eddy-turn-over time. For all of the cases $\phi_m = 0.5$ and $\sigma = 1$.

decreases the tendency of the particle to adjust to the gas temperature fluctuations. The rms temperature difference ($\overline{(T-T_p)'_{rms}}$), however, exhibits the opposite trend as observed in Fig. 9(b). The rms temperature difference markedly decreases in two-way coupling cases due to the modification of the gas temperature by the particles. An increase of σ results in a larger temperature difference as more heat transfer is needed to change the temperature of a particle having a larger heat capacity.

In Fig. 8(b) and 9(a), variations of $\overline{\langle\langle v^2\rangle\rangle}/\overline{\langle u^2\rangle}$ and $\overline{T'_{prms}}/\overline{T'_{rms}}$, respectively, were considered vs. τ_p where different behaviors for cases with one- and two-way couplings were observed. In Fig. 10, variations of $\overline{\langle\langle v^2\rangle\rangle}/\overline{\langle u^2\rangle}$ and $\overline{T'_{prms}}/\overline{T'_{rms}}$ are portrayed vs. $\tau_p/\bar{\tau}_e$. It is observed in the figure that by normalizing the particle time constant with the eddy-turn-over time, the data from one- and two-way coupling cases fall (nearly) on the same curve. Recall that a similar behavior was previously observed for the velocity autocorrelation curves when the time axis was normalized by the eddy-turn-over time (cf. Fig. 6(b)). This indicates that modifications in turbulence scales by the particles are the main cause of the observed changes in the statistics of the particles in two-way coupling and that a proper normalization may result in a unification of one- and two-way coupling results.

From a statistical point of view, of great interest is the relation between the fluctuations of thermodynamic variables. A common approach is to relate the fluctuating values of density, temperature, and pressure through a polytropic coefficient [21]. The local values of the polytropic coefficient is not well-defined as it is possible that the fluctuating density or the fluctuating pressure independently take zero values. To remove the singularity, Blaisdell et al. [6] propose an average value for the polytropic coefficient:

$$n = \frac{p'_{rms}/\langle p\rangle}{\rho'_{rms}/\langle\rho\rangle}. \tag{14}$$

The time averaged values of n are shown in Fig. 11 for different values of the mass loading ratio, the particle time constant, and the particle specific heat. In the absence of particles, the flow behaves very similarly to an isentropic flow with $n = \gamma = 1.4$. However, after the particles are

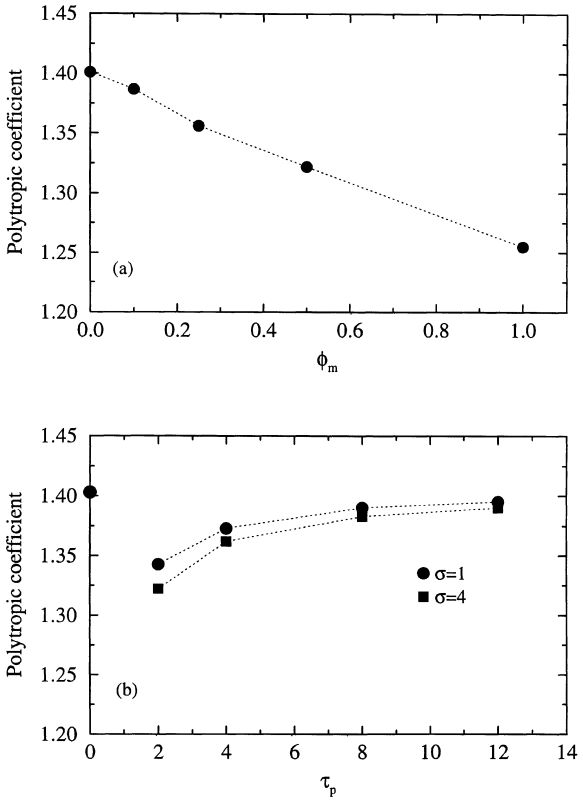

Fig. 11. Variations of the polytropic coefficient vs. (a) the mass loading ratio and (b) the particle time constant.

added to the flow the polytropic coefficient takes values smaller than 1.4 indicating deviations from an isentropic flow. This is expected as the heat transfer between the particles and the gas takes place at finite temperature differences and the reversibility condition is not satisfied. Interestingly, the polytropic coefficient decreases linearly with the increase of the mass loading ratio (Fig. 11(a)). In other words, for constant τ_p (or equivalently constant heat capacity), n varies linearly with the number of particles. The variations of the polytropic coefficient with the particle time constant (Fig. 11(b)), however, is non-linear as in this case both the number of particles and their heat capacity are variable. The increase of σ results in the decrease of n for all of the particle time constants. This is due to the increase of the heat transfer between the particles and the flow when the particle specific heat is increased.

Preferential distribution of particles in a turbulent flow has been the subject of many investigations in recent years (see [22] for a recent review). In the DNS of stationary incompressible turbulence, Squires and Eaton [20] show the tendency of particles to concentrate in the low vorticity and high strain rate regions of the flow. Similar to [20], here we consider the variation of the expected value of the particle number density conditioned on the parameter

$$II_d = \tfrac{1}{2}(S^2 - \tfrac{1}{4}\omega_i\omega_i) \tag{15}$$

which is related to the vorticity and the magnitude of the symmetric rate of strain tensor (S^2). In incompressible flows, II_d represents the second invariant of the deformation tensor. For a compressible flow, II_d does not have an analogous physical significance; however, it may still be used for flow characterization as the negative and positive values of II_d correspond to high strain rate and high vorticity regions of the flow, respectively. The number density (n_c) of the particles is calculated in a manner similar to that of the source term in the gas equations. At each grid point the total number of particles within a cell volume (δV) centered at the grid point is divided by the volume of the cell.

Figure 12(a) shows the variations of $\langle n_c|II_d\rangle/\langle n_c\rangle$ vs. II_d/II_{drms} for different values of the particle time constant and the mass loading ratio from the 64^3 simulations. The trends are similar to those previously observed in incompressible flow [20]—the particles indicate a higher

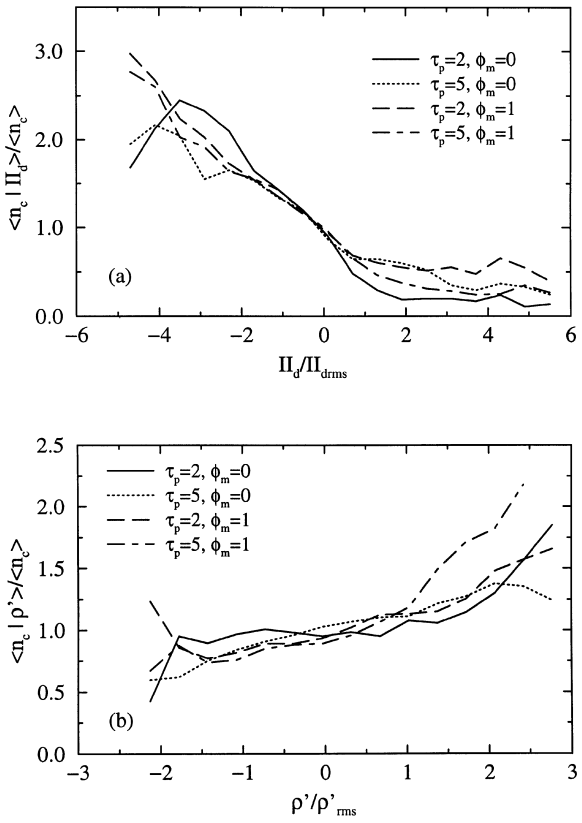

Fig. 12. Variations of the expected value of the particle number density conditioned on (a) the parameter II_d and (b) the gas fluctuating density.

Table 5
Correlation coefficients between the particle number density and carrier phase variables from the 64^3 simulations

	$\tau_p = 2$		$\tau_p = 5$	
	$\phi_m = 0$	$\phi_m = 1$	$\phi_m = 0$	$\phi_m = 1$
$\widehat{n_c II_d}$	−0.207	−0.166	−0.164	−0.143
$\widehat{n_c \rho'}$	0.035	0.064	0.017	0.081

tendency to accumulate in the regions of the flow with negative II_d. This is due to the centrifuging effects as indicated by previous investigations [20, 23]. Shown in Fig. 12 is also the particle concentration conditioned with the carrier phase density fluctuations. The particles exhibit a tendency to concentrate in the regions of the flow with higher density. These observations are also verified by comparing the values of the correlation coefficients given in Table 5. The correlation coefficient between the particle number density and a variable ψ is defined as $\widehat{n_c \psi} = (\langle n_c \psi \rangle / n_{crms} \psi_{rms})$ where $\psi = II_d$ or ρ'. Both Fig. 12 and Table 5 indicate that, for cases considered here, the tendency of particles to accumulate in high density regions is less than their preference to concentrate in high strain rate regions of the flow.

5. Conclusions

Dispersion of solid particles in forced low-Mach-number turbulent flows is investigated. The formulation utilized for this study describes the two-way coupling between the carrier and the dispersed phase in a realistic manner. The carrier phase is treated in the Eulerian frame and is simulated via DNS whereas the particles are tacked in a Lagrangian manner. The feasibility of a quasi-stationary turbulence by forcing the low wavenumbers of the flow is discussed, and it is shown that while the mean temperature increases in time, the statistics of the temperature fluctuations becomes stationary after an initial transient time.

The simulation results are used to study the effects of the particle time constant, the mass loading ratio, and the particle specific heat on the statistics of both phases in quasi-stationary turbulence. The temporal oscillations of the pressure–dilatation correlation is significantly damped in the presence of particles. This damping effect increases with the decrease of the particle time constant at the same mass loading ratio. The particles exhibit significant effects on the statistics of the flow even for small mass loading ratios. The most sensitive flow parameter to the mass loading ratio is the rms dilatation which shows a decrease by about 50% from its single-phase value for a mass loading ratio of 0.1. While both the mean and the rms values of the Mach number decrease with the increase of the mass loading ratio, the ratio of the two is about 0.41 for all values of the mass loading ratio. This observation can have major implications in modeling of particle-laden low-Mach-number turbulent flows.

The autocorrelation coefficient of the particle velocity increases with the increase of the mass loading ratio. This is similar to previous observation in incompressible flows, and is due to turbulence modifications by the particles. The autocorrelations (nearly) collapse on a single curve when the time axis is normalized by the eddy-turn-over time for each case. The autocorrelation of the particle temperature fluctuations also increases with the increase of the mass loading ratio. This autocorrelation is also strongly affected by variations of the particle time constant and/or the particle specific heat, and increases with the increase of these parameters. A peak value is observed in the variations of the particle velocity variance (normalized with the fluid velocity variance) with the mass loading ratio. For all of the values of the particle time constant, two-way coupling increases the ratio of the particle velocity variance to that of the fluid. A similar behavior is observed for the temperature fluctuations. It is also shown that the ratio of the rms of the particle temperature fluctuations to that of the gas decreases with the increase of the particle specific heat.

The evaluation of the polytropic coefficient for various cases indicates deviations from an isentropic flow when the particles are present. Interestingly, the polytropic coefficient exhibits a linear decrease with the increase of the mass loading ratio. The decrease of the particle time constant and/or the increase of the particle specific heat decreases the polytropic coefficient. Consistent with previous findings in incompressible flow, particles are preferentially collected in the regions of high strain rate. They also show a tendency to accumulate in regions of the flow with higher density.

Acknowledgments

Acknowledgment is made to the Donors of The Petroleum Research Fund, administered by the American Chemical Society, for partial support of this research. Computational resources for this work were in part provided by the San Diego Supercomputing Center and the College of Engineering Computer Facility at the University of Hawaii at Manoa.

References

[1] G.M. Faeth, Mixing, transport and combustion in sprays, Prog. Energy Combust. Sci. 13 (1987) 293–345.

[2] C. Crowe, T. Troutt, J. Chung, Numerical models for two-phase turbulent flows, Ann. Rev. Fluid Mech. 28 (1996) 11–43.
[3] G.I. Taylor, Diffusion by continuous movements, Proc. Lond. Math. Soc. 20 (2) (1921) 196–211.
[4] S. Corrsin, Turbulent flow, American Scientist 49 (1961) 300–324.
[5] F. Mashayek, F.A. Jaberi, R.S. Miller, P. Givi, Dispersion and polydispersity of droplets in stationary isotropic turbulence, Int. J. Multiphase Flow 23 (2) (1997) 337–355.
[6] G.A. Blaisdell, N.N. Mansour, W.C. Reynolds, Numerical simulation of compressible homogeneous turbulence, Department of Mechanical Engineering Report TF-50, Stanford University, Stanford, Ca, 1991.
[7] S. Lee, S.K. Lele, P. Moin, Eddy shocklets in decaying compressible turbulence, Phys. Fluids A 3 (4) (1991) 657–664.
[8] S. Kida, S. Orszag, Energy and spectral dynamics in forced compressible turbulence, Journal of Scientific Computing 5 (2) (1990) 85–125.
[9] S. Kida, S. Orszag, Energy and spectral dynamics in decaying compressible turbulence, Journal of Scientific Computing 7 (1) (1992) 1–34.
[10] H. Miura, S. Kida, Acoustic energy exchange in compressible turbulence, Phys. Fluids 7 (7) (1995) 1732–1742.
[11] M. Samimy, S.K. Lele, Motion of particles with inertia in a compressible free shear layer, Phys. Fluids 3 (8) (1991) 1915–1923.
[12] F. Mashayek, Direct numerical simulations of evaporating droplet dispersion in forced low Mach number turbulence, Int. J. Heat Mass Transfer 41 (17) (1998) 2601–2617.
[13] C.T. Crowe, M.P. Sharma, D.E. Stock, The particle-source in cell (PSI-cell) model for gas-droplet flows, J. Fluids Eng. 6 (1977) 325–332.
[14] G.B. Wallis, One Dimensional Two Phase Flow, McGraw-Hill, New York, 1969.
[15] R.B. Bird, W.E. Stewart, E.N. Lightfoot, Transport Phenomena, Wiley, New York, 1960.
[16] F. Mashayek, Droplet-turbulence interactions in low-Mach-number homogeneous shear two-phase flows, J. Fluid Mech. 376 (1998) 163–203.
[17] P. Givi, C.K. Madnia, Spectral methods in combustion, in: T.J. Chung (Ed.), Numerical Modeling in Combustion, chap. 8, Taylor and Francis, Washington, DC, 1993, pp. 409–452.
[18] V. Eswaran, S.B. Pope, An examination of forcing in direct numerical simulations of turbulence, Computers and Fluids 16 (3) (1988) 257–278.
[19] S. Elghobashi, G.C. Truesdell, On the two-way interaction between homogeneous turbulence and dispersed solid particles. I: turbulence modification, Phys. Fluids 5 (7) (1993) 1790–1801.
[20] K.D. Squires, J.K. Eaton, Particle response and turbulence modification in isotropic turbulence, Phys. Fluids 2 (1990) 1191–1203.
[21] M.W. Rubesin, A one-equation model of turbulence of use with the compressible Navier–Stokes equations, NASA Tech. Mem. X-73, 1976, p. 128.
[22] J.K. Eaton, J.R. Fessler, Preferential concentration of particles by turbulence, Int. J. Multiphase Flow Suppl. 20 (1994) 169–209.
[23] F. Wen, N. Kamalu, J.N. Chung, C.T. Crowe, T.T. R, Particle dispersion by vortex structures in plane mixing layers, J. Fluids Eng. 114 (1992) 657–666.